Room-Temperature Generation and Electric-Current-Driven Manipulation of Isolated Fractional Antiskyrmions in a Chiral Magnet

Zhidong He,[1,2] Zhan Wang,[1,2] Yunxiang Yang,[1,3] Yunchi Zhao,[1] Jun Shen,[4]
Tongyun Zhao,[1,2] Ying Zhang,[1,2,*] and Bao-gen Shen[1,2,5]

[1]*Beijing National Laboratory for Condensed Matter Physics, Institute of Physics, Chinese Academy of Sciences, Beijing 100190, China*
[2]*School of Physical Sciences, University of Chinese Academy of Sciences, Beijing 101408, China*
[3]*Anhui Provincial Key Laboratory of Magnetic Functional Materials and Devices, School of Materials Science and Engineering, Anhui University, Hefei 230601, China*
[4]*Department of Energy and Power Engineering, School of Mechanical Engineering, Beijing Institute of Technology, Beijing 100081, China*
[5]*Ningbo Institute of Materials Technology and Engineering, Chinese Academy of Sciences, Ningbo, Zhejiang, 315201, China*

(Received 30 April 2026; accepted 27 August 2026; published 15 September 2026)

Topologically protected (anti)skyrmions are promising information carriers for next-generation spintronics. Their fractional counterparts, however, have so far been observed only in bound pairs or lattice states, leaving a major challenge for the stabilization and electrical manipulation of an isolated fractional topological spin texture. Here, we report the generation of an isolated meron with half topological charge ($Q = 1/2$) and its electric-current-driven linear motion at room temperature in the chiral magnet $Mn_{1.4}PtSn$. Both Lorentz transmission electron microscopy and micromagnetic simulations provide evidence for the emergence of a unique fractional topological state due to the edge-induced topological transformation, distinct from bulk excitations. Importantly, the sample edge simultaneously acts as a one-dimensional track that enables robust current-driven linear motion by compensating the transverse Magnus force, thereby completely suppressing the intrinsic skyrmion Hall effect. These results establish an experimental pathway for generating and manipulating isolated fractional topological spin textures in real space, thereby offering a platform to explore fractional topological physics and spintronic functionalities.

DOI: 10.1103/lv79-x666

A variety of topologically protected particlelike spin textures, including (anti)skyrmions [1–4], merons [5–11], and hopfions [12,13] have been identified in magnetic materials. Owing to their nanoscale size, topological stability, and current-driven mobility at low electric current densities, these spin textures are regarded as promising information carriers for high-density, low-power magnetic memories [14–16], logic devices [17], and neuromorphic spintronic devices [18,19]. The correlated unique physics underlying these functionalities originates from their nontrivial spin topology [20], which can be quantitatively characterized by the topological charge, $Q = (1/4\pi)\iint \boldsymbol{n} \cdot [(\partial \boldsymbol{n}/\partial x) \times (\partial \boldsymbol{n}/\partial y)]\, dx\, dy$ [20]. Integer-charge objects such as (anti)skyrmions ($Q = 1$) have been experimentally confirmed to be able to stabilize either in the isolated or lattice states. Their electric manipulation behavior [14,21–26], together with the emergent magnetoelectric physics such as topological Hall effect [27] and skyrmion Hall effect [28], have laid the foundation for topological spintronics. The fractional excitations, as exemplified by the fractional quantum Hall effect, have represented a hallmark emergent phenomena in condensed-matter physics and their existences have been confirmed in strong correlation with sample surfaces, edges, or boundaries [29,30]. Similarly, the geometric confinement and disrupted translational continuity near the edges of magnetic systems are anticipated to stabilize distinctive real-space spin textures bearing fractional topological charges [31,32]. However, these fractional topological spin textures have only been experimentally discovered in the form of pair states [5,6,8–10,33–36] or in lattice configurations [7,37–39] with total integer charge and without successful electric manipulation.

Therefore, the experimental creation and electric control of an isolated fractional topological spin texture would represent critical advances for fundamental understanding of the fractional topological physics and spintronic applications, yet remain an outstanding challenge. Herein, we present a comprehensive study on the generation and current-driven behavior of an isolated meron ($Q = 1/2$) in the chiral magnet $Mn_{1.4}PtSn$ via integrating Lorentz transmission electron microscopy (LTEM) observations with systematic micromagnetic simulations. We find that when an external magnetic field drives the topological

*Contact author: zhangy@iphy.ac.cn

 © 2026 American Physical Society

transformation of an integer antiskyrmion near the sample edge, the broken continuity of the spin texture stabilizes this unique isolated half antiskyrmion state. Notably, the sample edge also acts as a naturally one-dimensional track to guide the linear motion of this meron, completely suppressing the transverse drift induced by intrinsic skyrmion Hall effect. The robustness of fractional spin textures during generation and manipulation over a broad temperature range and without requiring magnetic field reveals striking parallels to spintronic applications.

The spin configuration of antiskyrmion carrying integer topological charge $Q = 1$ [Fig. 1(a)] is determined by the anisotropic Dzyaloshinskii-Moriya interaction (DMI) due to the intrinsic symmetry-broken D_{2d} crystal structure of chiral $Mn_{1.4}PtSn$ [4,25,40,41]. According to theoretical prediction [32], when an antiskyrmion approaches and interacts with the sample edge, the reconstruction of interrupted spin field drives the transformation of an integer topological texture into exotic topological edge states [Figs. 1(b) and 1(c)]. To further explore the unique features of this fractional edge state, we use focused ion beam (FIB) milling to fabricate $Mn_{1.4}PtSn$ thin plates with the stripe domains oriented perpendicular or parallel to the sample edge and Pt electrodes deposited at the microdevice ends (for details, see Supplemental Material Figs. S1–S3 [42]). Possible Ga ion-induced damage has been minimized by adopting PtCx protective layer and low-energy FIB milling procedures during sample preparation, ensuring high-quality LTEM imaging of the edge state [52].

By systematically analyzing the magnetic domain contrast at underfocus [Fig. 1(d)] and overfocus [Fig. 1(e)] conditions ($\Delta z = 250$ μm), the in-plane magnetization distribution is reconstructed using the transport-of-intensity equation (TIE) method [44] (Supplemental Material Fig. S4 [42]). The reconstructed spin texture as shown in Fig. 1(f) is identified as an isolated meron with fractional topological charge of $Q = 1/2$, in good agreement with the theoretical meron spin configuration and simulated LTEM images (Supplemental Material Fig. S5 [42]). Further off-axis electron holography reveals the in-plane magnetic induction maps and the

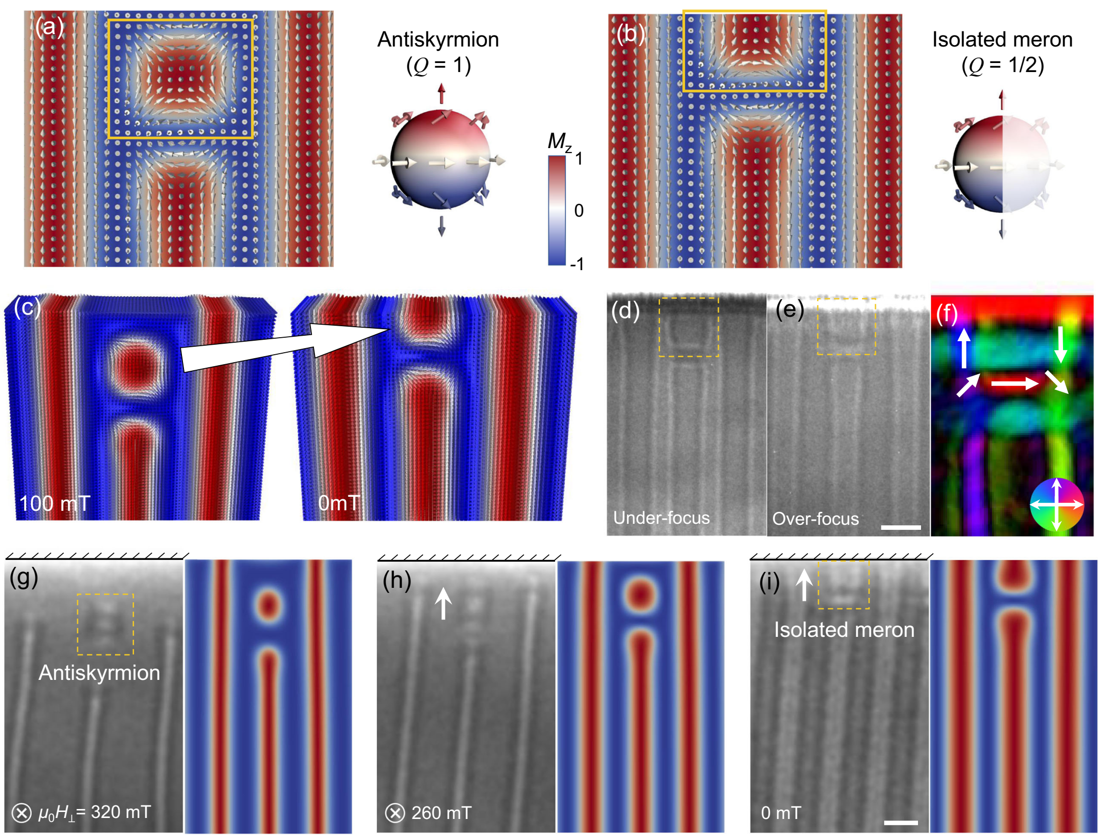

FIG. 1. Edge-induced topological transition and stabilization of an isolated meron at room temperature in chiral $Mn_{1.4}PtSn$ magnet. (a) Simulated antiskyrmion with topological charge $Q = 1$. (b) Simulated isolated edge state with fractional topological charge $Q = 1/2$, corresponding to half-antiskyrmion spin winding. (c) Simulated topological transformation from an integer to fractional antiskyrmion due to the demagnetizing fields and edge-induced spin reconstruction under open boundary conditions. (d),(e) Fresnel LTEM images showing the domain contrast of an isolated fractional edge state at underfocus and overfocus conditions ($\Delta z = 250$ μm), respectively. (f) Identification of an isolated meron using reconstructed in-plane magnetization distribution. (g)–(i) LTEM images and corresponding simulations showing the edge-induced transformation from an integer antiskyrmion into an isolated meron while reducing the magnetic field from 320 mT to zero field. The direction of decreasing magnetic field is marked out. Scale bar, 100 nm.

reconstructed phase distributions consistent with LTEM results (Supplemental Material Fig. S6 [42]). The disappearance of the upper Bloch line in antiskyrmions indicates a hallmark signature of an isolated meron generation at the edge when the magnetic field decreases to around 120 mT (Supplemental Material Figs. S6 and S7 [42]). Moreover, this one-dimensional edge facilitates the self-assembly of fractional spin textures into ordered meron molecules, including dimers and higher-order clusters (Supplemental Material Fig. S8 [42]). Micromagnetic simulations reveal that the edge-mediated antiskyrmion-to-meron transformation exhibits remarkable robustness across a thickness range of about 50–200 nm (Supplemental Material Fig. S9 [42]), thereby accommodating the inherent thickness variations associated with FIB fabrication.

The generation and stability of this isolated meron are governed by the interplay between edge-induced chiral distortion and demagnetizing fields. At the edge of a finite-size magnetic sample, the abrupt loss of full atomic coordination gives rise to uncompensated DMI bonds, leading to characteristic edge-twisted spin textures [53]. The presence of the sample edge breaks the closed-mapping condition required for an integer topological charge and renders the fractional topological states energetically more favorable than fully integer antiskyrmions under low magnetic fields. As the magnetic field decreases, an antiskyrmion located near the edge becomes unstable and then the spin texture becomes deformed by edge potential, undergoing topological transition into an isolated meron, which remains stable even at zero field [Figs. 1(g)–1(i)]. The topological transition can be analogous to vortex detachment at superfluid boundaries [54] or skyrmion generation from magnetic stripes [22,55]. In contrast to the randomly fractionalized parts cut from an entire magnetic texture due to the geometric termination [14,45,46], the isolated meron quasiparticles transformed from an integer antiskyrmion exhibits well-defined morphology, robust stability, and current-driven dynamics. This edge-mediated topological transition cannot occur inside the bulk because a fairly high energy is required to create an isolated meron from uniform sample. The stabilized fractional topological states over broad temperature and field range (Supplemental Material Fig. S10 [42]) further highlight their potential spintronic applications as topological information units.

We next investigate the current-driven dynamics of an isolated meron under the electric current pulse applied parallel to the nanodevice. The displacement of the isolated meron as a function of pulse number and current density is shown in Fig. 2. Meron motion is initiated along the electron-flow direction only when the current density exceeds a critical threshold of $j_c = 1.2 \times 10^6$ A cm^{-2} [Fig. 2(a)], marking the onset of depinning. The meron exhibits creeplike motion at about $j_e = 1.4 \times 10^6$ A cm^{-2}, followed by a pronounced velocity increase at $j_e = 1.9 \times 10^6$ A cm^{-2} [Fig. 2(b)]. Above this threshold, the meron enters a steady-flow

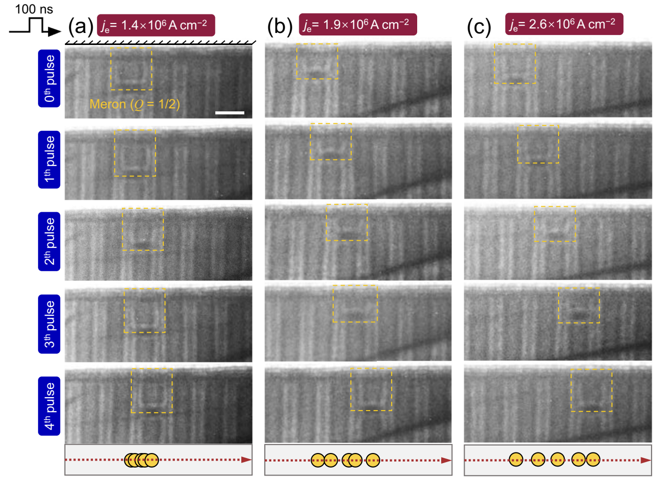

FIG. 2. Electric current-driven linear motion of an isolated meron at room temperature and zero magnetic field in a $Mn_{1.4}PtSn$ microdevice. (a)–(c) Sequential LTEM images showing the displacement of an isolated meron under parallel electric current pulses with pulse width of $\tau = 100$ ns. Columns for the increase of the pulse numbers and rows for the increase of electric current densities. The meron remains pinned below the critical current density j_c and then enters a creeplike motion after depinning, finally following steady linear motion at higher current densities. Yellow boxes mark the position change of one isolated meron. Scale bar, 100 nm.

regime in which the velocity increases nearly linearly with current density [Fig. 2(c) and Supplemental Movie 1 [42]]. Its trajectory remains strictly one dimensional with no discernible transverse deflection, demonstrating the complete suppression of the intrinsic skyrmion Hall effect. From the linear regime of Fig. 3(a), we extract a mobility of 3.6×10^{-11} m^3(A s)$^{-1}$, comparable to the reported values for skyrmions in chiral magnets [56–58]. When the electric current density is higher than $j_e = 3.8 \times 10^6$ A cm^{-2}, the isolated meron tends to annihilate at the edge due to the significant Joule heating effects.

Notably, the linear meron motion is observed only at one electric current direction. If the direction of electric current is reversed, the isolated meron would rapidly annihilate at the sample edge, which will be discussed later. The dependence of meron velocity on current density follows the standard depinning relation $v \propto \sqrt{j_e - j_c}$ as shown in Fig. 3(a), indicating that the driving force is governed by the current-induced spin-transfer-torque (STT) [59]. The pulse width τ also has a pronounced effect on depinning and the critical current density j_c is lower while increasing the pulse width [Fig. 3(b)] due to the accumulated thermal effects. The electric driving threshold for depinning is reduced to $j_e = 5.1 \times 10^5$ A cm^{-2} at pulse width $\tau = 2000$ ns. By contrast, the shorter pulses allow the higher current density, thereby enabling faster meron motion. A velocity of ~ 1 m s^{-1} is obtained for $\tau = 100$ ns, whereas a much higher velocity of ~ 17 m s^{-1} is reached for $\tau = 6$ ns.

Micromagnetic simulations indicate that a fieldlike out-of-plane torque can efficiently drive the linear motion of isolated meron along the sample edge while preserving its topological integrity [Fig. 3(c)].

We adopt the collective coordinate approximation for the rigid topological spin textures and describe the STT-driven dynamics using the Thiele equation:$\mathbf{G} \times (\mathbf{v}^{(s)} - \mathbf{v}^{(d)}) + \mathcal{D}(\beta \mathbf{v}^{(s)} - \alpha \mathbf{v}^{(d)}) + \mathbf{F}_A = 0$, where $\mathbf{v}^{(d)}$ is meron velocity, $\mathbf{v}^{(s)} = -(gP\mu_B/2eM_s)\mathbf{j} = b\mathbf{j}$ is electron drift velocity induced by the spin-polarized current. Here, $\mathbf{G} = 4\pi Q e_z$ is the gyrovector associated with the Magnus force F_M. For skyrmions with an integer topological charge $Q = 1$, the gyroscopic term is dominant and gives rise to a pronounced skyrmion Hall effect [14,28]. For an isolated meron with a reduced topological charge $Q = 1/2$, the magnitude of the gyrovector is reduced by half. Nevertheless, a transverse deflection is still expected in principle with the approximate Hall angle $\theta_H \approx \arctan\{(\alpha - \beta)[\eta/Q]\}$ (for details, see Supplemental Material Sec. S1 [42]).

Systematic micromagnetic simulations reveal that the linear motion of an isolated meron under electric current-driven dynamics arises from the synergistic interplay between the STT-induced driving force, the topological Magnus response, and the edge-induced attractive interaction. The edge-induced demagnetizing fields drive the magnetization near the edge away from the bulk configuration and promote the formation of flux-closure-like spin arrangements, which favors the attraction of topological spin textures toward the sample edge. The straight trajectory arises from a balance between the edge-induced attractive force (F_A) and the Magnus force (F_M) [Fig. 3(c)] for an isolated meron along the sample edge, which is different from the repulsive force to balance the intrinsic Magnus force for integer textures [25,52].

Theoretically, the resulting transverse dynamics sensitively depend on the difference between the Gilbert damping and nonadiabatic spin-transfer torque parameters $(\alpha - \beta)$. Here, α is fixed at a representative value of 0.1, whereas the parameter β is varied to tune the balance between competing forces. Micromagnetic simulations show that the transverse Magnus force is insufficient to counteract the edge attraction for $0.10 \leq \beta \leq 0.13$, causing the meron to move toward the boundary and undergo continuous topological annihilation from 1/2 to 0 [Fig. 3(d)]. By contrast, nearly linear motion along the sample edge emerges for $0.14 \leq \beta \leq 0.16$, where the

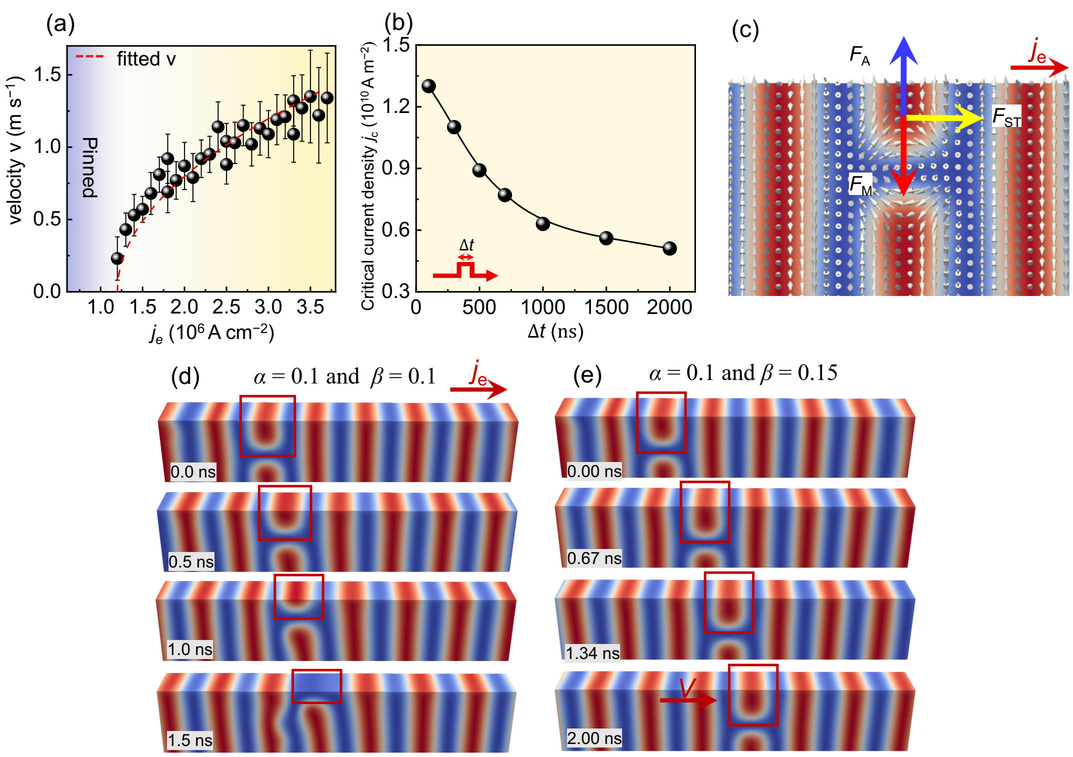

FIG. 3. Current-driven dynamics of an isolated meron and the mechanism illustration for linear motion. (a) Averaged velocity of an isolated meron as a function of current density, following $v \propto \sqrt{j_e - j_c}$ dependence, consistent with standard depinning theory. (b) Dependence of the critical current density j_c on pulse width. (c) Schematic illustration on the linear motion mechanism of an isolated meron based on the competition between the Magnus force (F_M) and the edge-induced attractive force (F_A). The spin-transfer torque (F_{ST}) provides the longitudinal driving force. (d) Micromagnetic simulations showing the current-driven dynamics of an isolated meron at nanosecond scale with $\alpha = 0.1$ and $\beta = 0.1$, and (e) with $\alpha = 0.1$ and $\beta = 0.15$. The meron position is marked by red boxes, and the color represents the magnetization directions.

Magnus force is approximately balanced by the edge-induced attraction [Fig. 3(e)]. When $\beta > 0.16$, the Magnus force becomes dominant, driving the meron away from the edge and into the sample interior, accompanied by a pronounced elongation of the spin texture. Notably, reversing the current direction reverses the Magnus force but remains the attractive force, directing the meron toward the edge and triggering rapid annihilation. This asymmetric response under opposite current directions distinguishes the present system from conventional geometric-confined skyrmion systems [14,21,60]. The combination of reduced Magnus force due to fractional topology and the attractive interaction between meron and sample edge establishes unique electric driven behavior (Supplemental Material Fig. S11 [42]).

Beyond the case of an isolated meron embedded in perpendicular stripe domains, we further study the dynamics when confined within parallel stripe domains near the edge [Fig. 4(a)]. In this case, both the attraction force from the sample edge and the repulsion force from stripe confinement contribute to canceling the Magnus force. Remarkably, as the isolated meron is driven under the electric current, the trailing (leading) stripe segments undergo local stretching (contraction) through magnetization rotation, while the overall helical background remains immobile (Supplemental Movie 2 [42]). This distinctive current response provides strong evidence for the solitonic nature of the isolated meron and is further confirmed by micromagnetic simulations (Supplemental Material Fig. S12 [42]). Moreover, the velocity-current characteristics of the meron in parallel stripes are comparable to those observed in perpendicular stripe domains (Supplemental Material Fig. S13 [42]). However, more pronounced displacement coupled with the meron motion is easier to be visualized for the perpendicular stripe background in contrast with that for the parallel stripe configuration due to their different magnetization response relative to the electric current direction. Notably, meron molecules, including dimers ($Q = 1$) [Fig. 4(b)] and higher-order bound states ($Q = 3/2$) undergo robust collective linear motion under electric currents, while preserving the relative internal configuration of the meron molecules during movement [Figs. 4(b) and 4(c) and Supplemental Movie 3 [42]]. This behavior is sharply different with the desynchronized dynamics of skyrmion chains in a ferromagnetic background [60].

In conclusion, we have systematically investigated the generation and current-driven linear motion of isolated fractional spin textures by exploiting the unique contribution of the sample edge. The broken translational continuity and demagnetization field at the edge plays a crucial role in stabilizing fractional spin textures, which are fundamentally distinct from the integer topological objects. The intrinsic skyrmion Hall effect is completely suppressed by the counterbalance between the edge-induced attraction force and transverse Magnus force, enabling the controlled motion along the edge. The unique dynamics of the isolated fractional topological excitations at room temperature without requiring magnetic field establish an experimental platform for exploring underlying physics and potentials as information carriers in spintronic devices.

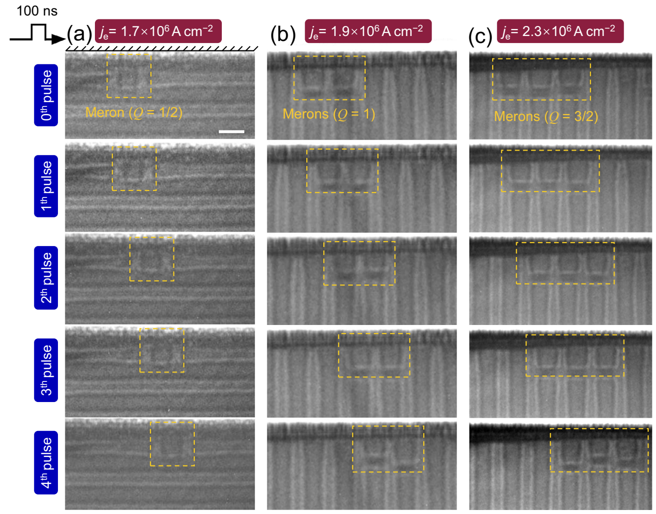

FIG. 4. Electric current-driven collective motion of meron molecules, including dimers and higher-order clusters. (a) Sequential LTEM images showing the displacement of an isolated meron embedded within parallel helical stripe domains under sequential current pulses of $j_e = 1.7 \times 10^6$ A cm^{-2}. The meron motion is accompanied by local stretching (contraction) of the stripe segments, while the helical background remains essentially immobile. Collective current-driven motion of meron molecules at room temperature and zero magnetic field, including (b) meron dimers ($Q = 1$) and (c) higher-order meron cluster with ($Q = 3/2$). Yellow boxes mark the meron positions. Scale bar, 100 nm.

Acknowledgments—This work was supported by the National Natural Science Foundation of China (No. 52525108, No. 52271195, No. 52130103, No. 52601435), the Creative Research Group Project of the National Science Foundation of China (Grant No. 52688201), the National Key R&D Program of China (Grant No. 2024YFA1611301), the CAS Project for Young Scientists in Basic Research (No. YSBR-084), and the Postdoctoral Fellowship Program and China Postdoctoral Science Foundation (No. BX20250164).

Data availability—There are no publicly available research data or software supporting this manuscript. Requests for further information or data should be sent to the authors.

[1] A. N. Bogdanov and D. Yablonskii, Thermodynamically stable "vortices" in magnetically ordered crystals. The mixed state of magnets, Zh. Eksp. Teor. Fiz. **95**, 178 (1989).
[2] S. Mühlbauer, B. Binz, F. Jonietz, C. Pfleiderer, A. Rosch, A. Neubauer, R. Georgii, and P. Böni,

Skyrmion lattice in a chiral magnet, Science **323**, 915 (2009).

[3] X. Yu, Y. Onose, N. Kanazawa, J. H. Park, J. Han, Y. Matsui, N. Nagaosa, and Y. Tokura, Real-space observation of a two-dimensional skyrmion crystal, Nature (London) **465**, 901 (2010).

[4] A. K. Nayak, V. Kumar, T. Ma, P. Werner, E. Pippel, R. Sahoo, F. Damay, U. K. Rossler, C. Felser, and S. S. P. Parkin, Magnetic antiskyrmions above room temperature in tetragonal Heusler materials, Nature (London) **548**, 561 (2017).

[5] C. Phatak, A. K. Petford-Long, and O. Heinonen, Direct observation of unconventional topological spin structure in coupled magnetic discs, Phys. Rev. Lett. **108**, 067205 (2012).

[6] S. Wintz, C. Bunce, A. Neudert, M. Körner, T. Strache, M. Buhl, A. Erbe, S. Gemming, J. Raabe, C. Quitmann, and J. Fassbender, Topology and origin of effective spin meron pairs in ferromagnetic multilayer elements, Phys. Rev. Lett. **110**, 177201 (2013).

[7] X. Yu, W. Koshibae, Y. Tokunaga, K. Shibata, Y. Taguchi, N. Nagaosa, and Y. Tokura, Transformation between meron and skyrmion topological spin textures in a chiral magnet, Nature (London) **564**, 95 (2018).

[8] N. Gao, S.-G. Je, M.-Y. Im, J. W. Choi, M. Yang, Q.-c. Li, T. Wang, S. Lee, H.-S. Han, and K.-S. Lee, Creation and annihilation of topological meron pairs in in-plane magnetized films, Nat. Commun. **10**, 5603 (2019).

[9] Y. Gao, Q. Yin, Q. Wang, Z. Li, J. Cai, T. Zhao, H. Lei, S. Wang, Y. Zhang, and B. Shen, Spontaneous (anti)meron chains in the domain walls of van der Waals ferromagnetic $Fe_{5-x}GeTe_2$, Adv. Mater. **32**, 2005228 (2020).

[10] T. Nagase, Y.-G. So, H. Yasui, T. Ishida, H. K. Yoshida, Y. Tanaka, K. Saitoh, N. Ikarashi, Y. Kawaguchi, and M. Kuwahara, Observation of domain wall bimerons in chiral magnets, Nat. Commun. **12**, 3490 (2021).

[11] H. Jani, J.-C. Lin, J. Chen, J. Harrison, F. Maccherozzi, J. Schad, S. Prakash, C.-B. Eom, A. Ariando, and T. Venkatesan, Antiferromagnetic half-skyrmions and bimerons at room temperature, Nature (London) **590**, 74 (2021).

[12] R. Voinescu, J.-S. B. Tai, and I. I. Smalyukh, Hopf solitons in helical and conical backgrounds of chiral magnetic solids, Phys. Rev. Lett. **125**, 057201 (2020).

[13] F. Zheng, N. S. Kiselev, F. N. Rybakov, L. Yang, W. Shi, S. Blügel, and R. E. Dunin-Borkowski, Hopfion rings in a cubic chiral magnet, Nature (London) **623**, 718 (2023).

[14] J. Iwasaki, M. Mochizuki, and N. Nagaosa, Current-induced skyrmion dynamics in constricted geometries, Nat. Nanotechnol. **8**, 742 (2013).

[15] S. Parkin and S.-H. Yang, Memory on the racetrack, Nat. Nanotechnol. **10**, 195 (2015).

[16] G. Gubbiotti, A. Barman, S. Ladak, C. Bran, D. Grundler, M. Huth, H. Plank, G. Schmidt, S. Van Dijken, and R. Streubel, 2025 roadmap on 3D nano-magnetism, J. Phys. Condens. Matter **37**, 143502 (2025).

[17] Y. Zhou, Magnetic skyrmions: Intriguing physics and new spintronic device concepts, Natl. Sci. Rev. **6**, 210 (2019).

[18] J. Grollier, D. Querlioz, K. Camsari, K. Everschor-Sitte, S. Fukami, and M. Stiles, Neuromorphic spintronics, National electronics review **3**, 360 (2020).

[19] C. H. Marrows, J. Barker, T. A. Moore, and T. Moorsom, Neuromorphic computing with spintronics, npj Spintron. **2**, 12 (2024).

[20] N. Nagaosa and Y. Tokura, Topological properties and dynamics of magnetic skyrmions, Nat. Nanotechnol. **8**, 899 (2013).

[21] J. Sampaio, V. Cros, S. Rohart, A. Thiaville, and A. Fert, Nucleation, stability and current-induced motion of isolated magnetic skyrmions in nanostructures, Nat. Nanotechnol. **8**, 839 (2013).

[22] W. Jiang, P. Upadhyaya, W. Zhang, G. Yu, M. B. Jungfleisch, F. Y. Fradin, J. E. Pearson, Y. Tserkovnyak, K. L. Wang, and O. Heinonen, Blowing magnetic skyrmion bubbles, Science **349**, 283 (2015).

[23] S. Woo, K. Litzius, B. Krüger, M.-Y. Im, L. Caretta, K. Richter, M. Mann, A. Krone, R. M. Reeve, and M. Weigand, Observation of room-temperature magnetic skyrmions and their current-driven dynamics in ultrathin metallic ferromagnets, Nat. Mater. **15**, 501 (2016).

[24] J. Müller, J. Rajeswari, P. Huang, Y. Murooka, H. M. Rønnow, F. Carbone, and A. Rosch, Magnetic skyrmions and skyrmion clusters in the helical phase of Cu_2OSeO_3, Phys. Rev. Lett. **119**, 137201 (2017).

[25] Z. He, Z. Li, Z. Chen, Z. Wang, J. Shen, S. Wang, C. Song, T. Zhao, J. Cai, and S.-Z. Lin, Experimental observation of current-driven antiskyrmion sliding in stripe domains, Nat. Mater. **23**, 1048 (2024).

[26] V. T. Pham, N. Sisodia, I. Di Manici, J. Urrestarazu-Larrañaga, K. Bairagi, J. Pelloux-Prayer, R. Guedas, L. D. Buda-Prejbeanu, S. Auffret, and A. Locatelli, Fast current-induced skyrmion motion in synthetic antiferromagnets, Science **384**, 307 (2024).

[27] A. Neubauer, C. Pfleiderer, B. Binz, A. Rosch, R. Ritz, P. G. Niklowitz, and P. Böni, Topological Hall effect in the A phase of MnSi, Phys. Rev. Lett. **102**, 186602 (2009).

[28] W. Jiang, X. Zhang, G. Yu, W. Zhang, X. Wang, M. Benjamin Jungfleisch, John E. Pearson, X. Cheng, O. Heinonen, K. L. Wang, Y. Zhou, A. Hoffmann, and S. G. E. te Velthuis, Direct observation of the skyrmion Hall effect, Nat. Phys. **13**, 162 (2016).

[29] D. C. Tsui, H. L. Stormer, and A. C. Gossard, Two-dimensional magnetotransport in the extreme quantum limit, Phys. Rev. Lett. **48**, 1559 (1982).

[30] R. B. Laughlin, Anomalous quantum Hall effect: An incompressible quantum fluid with fractionally charged excitations, Phys. Rev. Lett. **50**, 1395 (1983).

[31] S. A. Díaz, J. Klinovaja, and D. Loss, Topological magnons and edge states in antiferromagnetic skyrmion crystals, Phys. Rev. Lett. **122**, 187203 (2019).

[32] T. Hirosawa, S. A. Diaz, J. Klinovaja, and D. Loss, Magnonic quadrupole topological insulator in antiskyrmion crystals, Phys. Rev. Lett. **125**, 207204 (2020).

[33] M. Ezawa, Compact merons and skyrmions in thin chiral magnetic films, Phys. Rev. B **83**, 100408(R) (2011).

[34] F. P. Chmiel, N. Waterfield Price, R. D. Johnson, A. D. Lamirand, J. Schad, G. van der Laan, D. T. Harris, J. Irwin, M. S. Rzchowski, and C.-B. Eom, Observation of magnetic vortex pairs at room temperature in a planar α-Fe_2O_3/Co heterostructure, Nat. Mater. **17**, 581 (2018).

[35] M. Bhukta, T. Dohi, V. K. Bharadwaj, R. Zarzuela, M.-A. Syskaki, M. Foerster, M. A. Niño, J. Sinova, R. Frömter, and M. Kläui, Homochiral antiferromagnetic merons, antimerons and bimerons realized in synthetic antiferromagnets, Nat. Commun. **15**, 1641 (2024).

[36] K. Zhu, F. N. Rybakov, Z. Wang, W. Gao, S. Sun, W. Wang, J. Li, H. Tian, O. Eriksson, and H. Yang, Light-induced bimerons in a chiral magnet, Nat. Commun. **17**, 3185 (2026).

[37] S.-Z. Lin, A. Saxena, and C. D. Batista, Skyrmion fractionalization and merons in chiral magnets with easy-plane anisotropy, Phys. Rev. B **91**, 224407 (2015).

[38] N. Mukai and A. O. Leonov, Skyrmion and meron ordering in quasi-two-dimensional chiral magnets, Phys. Rev. B **106**, 224428 (2022).

[39] M. Cai, S. Wang, Y. Zhang, X. Bao, D. Shen, J. Ren, L. Qiu, H. Yu, Z. Luo, M. Kläui, S. Zhang, N. Jaouen, G. van der Laan, T. Hesjedal, K. Shen, and J. Zhang, Stabilization and observation of large-area ferromagnetic bimeron lattice, Phys. Rev. Lett. **135**, 116703 (2025).

[40] P. Vir, N. Kumar, H. Borrmann, B. Jamijansuren, G. Kreiner, C. Shekhar, and C. Felser, Tetragonal superstructure of the antiskyrmion hosting Heusler compound $Mn_{1.4}PtSn$, Chem. Mater. **31**, 5876 (2019).

[41] Y. Zhang, J. Liu, Y. Dong, S. Wu, J. Zhang, J. Wang, J. Lu, A. Rückriegel, H. Wang, and R. Duine, H. Yu, Z. Luo, K. Shen, and J. Zhang, Strain-driven Dzyaloshinskii-Moriya interaction for room-temperature magnetic skyrmions, Phys. Rev. Lett. **127**, 117204 (2021).

[42] See Supplemental Material at http://link.aps.org/supplemental/10.1103/lv79-x666 for details of sample preparation, magnetic characterization, micromagnetic simulations, and additional current-driven dynamics, which includes Refs. [43–51].

[43] R. Streubel, Phase contrast imaging of non-collinear spin textures with Lorentz microscopy, J. Mater. Res. **38**, 4977 (2023).

[44] K. Ishizuka and B. Allman, Phase measurement of atomic resolution image using transport of intensity equation, J. Electron Microsc. **54**, 191 (2005).

[45] A. Vansteenkiste, J. Leliaert, M. Dvornik, M. Helsen, F. Garcia-Sanchez, and B. Van Waeyenberge, The design and verification of MuMax3, AIP Adv. **4**, 107133 (2014).

[46] S. Zhang and Z. Li, Roles of nonequilibrium conduction electrons on the magnetization dynamics of ferromagnets, Phys. Rev. Lett. **93**, 127204 (2004).

[47] F. Zheng, F. N. Rybakov, N. S. Kiselev, D. Song, A. Kovács, H. Du, S. Blügel, and R. E. Dunin-Borkowski, Magnetic skyrmion braids, Nat. Commun. **12**, 5316 (2021).

[48] J. Iwasaki, M. Mochizuki, and N. Nagaosa, Universal current-velocity relation of skyrmion motion in chiral magnets, Nat. Commun. **4**, 1463 (2013).

[49] T. Schulz, R. Ritz, A. Bauer, M. Halder, M. Wagner, C. Franz, C. Pfleiderer, K. Everschor, M. Garst, and A. Rosch, Emergent electrodynamics of skyrmions in a chiral magnet, Nat. Phys. **8**, 301 (2012).

[50] C. Kind and D. Foster, Magnetic skyrmion binning, Phys. Rev. B **103**, L100413 (2021).

[51] Z. Zeng, C. Zhang, C. Jin, J. Wang, C. Song, Y. Ma, Q. Liu, and J. Wang, Dynamics of skyrmion bags driven by the spin–orbit torque, Appl. Phys. Lett. **117**, 172404EE (2020).

[52] H. Du, R. Che, L. Kong, X. Zhao, C. Jin, C. Wang, J. Yang, W. Ning, R. Li, and C. Jin, Edge-mediated skyrmion chain and its collective dynamics in a confined geometry, Nat. Commun. **6**, 8504 (2015).

[53] S. A. Meynell, M. N. Wilson, H. Fritzsche, A. N. Bogdanov, and T. L. Monchesky, Surface twist instabilities and skyrmion states in chiral ferromagnets, Phys. Rev. B **90**, 014406 (2014).

[54] N. A. Keepfer, G. W. Stagg, L. Galantucci, C. F. Barenghi, and N. G. Parker, Spin-up of a superfluid vortex lattice driven by rough boundaries, Phys. Rev. B **102**, 144520 (2020).

[55] S.-Z. Lin, Edge instability in a chiral stripe domain under an electric current and skyrmion generation, Phys. Rev. B **94**, 020402(R) (2016).

[56] J. Tang, Y. Wu, W. Wang, L. Kong, B. Lv, W. Wei, J. Zang, M. Tian, and H. Du, Magnetic skyrmion bundles and their current-driven dynamics, Nat. Nanotechnol. **16**, 1086 (2021).

[57] L. Peng, K. Karube, Y. Taguchi, N. Nagaosa, Y. Tokura, and X. Yu, Dynamic transition of current-driven single-skyrmion motion in a room-temperature chiral-lattice magnet, Nat. Commun. **12**, 6797 (2021).

[58] W. Wang, D. Song, W. Wei, P. Nan, S. Zhang, B. Ge, M. Tian, J. Zang, and H. Du, Electrical manipulation of skyrmions in a chiral magnet, Nat. Commun. **13**, 1593 (2022).

[59] S. Brazovskii and T. Nattermann, Pinning and sliding of driven elastic systems: From domain walls to charge density waves, Adv. Phys. **53**, 177 (2004).

[60] D. Song, W. Wang, S. Zhang, Y. Liu, N. Wang, F. Zheng, M. Tian, R. E. Dunin-Borkowski, J. Zang, and H. Du, Steady motion of 80-nm-size skyrmions in a 100-nm-wide track, Nat. Commun. **15**, 5614 (2024).